Journal of Applied Electrochemistry **34**: 477–486, 2004.

Transmission line modeling of the manganese dioxide electrode in concentrated KOH electrolytes

SCOTT W. DONNE[1,*] and JOHN H. KENNEDY[2]
[1]*Eveready Battery Company, Inc., 25225 Detroit Road, Westlake, OH 44145, USA*
[2]*Department of Chemistry, University of California, Santa Barbara, CA 93106, USA*
*(*author for correspondence, e-mail: scott.donne@newcastle.edu.au)*

Received 18 August 2003; accepted in revised form 17 December 2003

Key words: batteries, battery materials, electrochemical impedance spectroscopy, manganese dioxide

Abstract

A transmission line model describing the electrochemical impedance spectroscopy (EIS) behavior of the EMD electrode in concentrated KOH electrolytes has been developed. The model takes into consideration the various charge transport paths through the electrode. In general, it consists of parameters describing the electrical, electrochemical and geometric properties of the electrode. Arbitrary values were selected for these parameters and used to calculate the electrode impedance as a function of frequency. The trends in the calculated data were consistent with our physical picture of the electrode. Experimental EIS data from a previous study was modeled using the transmission line. The comparison between experimental and predicted data was excellent (<3% deviation).

1. Introduction

Zn/MnO_2 batteries are one of the most common power sources for portable electronic devices. These batteries can be divided into two broad categories based on the electrolyte used; i.e., Leclanché electrolytes ($ZnCl_2$–NH_4Cl) and concentrated alkaline (KOH) electrolytes. These cells are mainly used for primary applications; however, there is a small proportion of the market that is currently occupied by secondary Zn/MnO_2 cells. Those that employ a concentrated alkaline electrolyte are preferred because of their superior electrochemical characteristics.

The performance of the manganese dioxide electrode is of prime importance in determining the success of commercial Zn/MnO_2 cells. This is the result of a unique combination of its physicochemical, electrochemical and economic properties. Over the past 50 years a vast amount of research has been carried out in both academic and industrial laboratories with the goal of obtaining more information and improving the performance of the manganese dioxide electrode. This study will focus on the manganese dioxide electrode in concentrated alkaline electrolytes.

There are numerous crystal forms of manganese dioxide that have been investigated for electrochemical performance, and hence their suitability for use in commercial cells. The majority have at least some electrochemical activity, but the γ-MnO_2 variety has been found to be the most suitable. γ-MnO_2 can be found in a number of natural deposits, or it can be produced synthetically using either electrochemical or chemical procedures. Of these, electrodeposited γ-MnO_2 (EMD) has been found to be most suited for use in alkaline Zn/MnO_2 cells and hence it will be the subject of this study. In simple terms, γ-MnO_2 can be described as an intergrowth between the pyrolusite (β-MnO_2) and ramsdellite varieties of manganese dioxide. In reality, however, the structure of γ-MnO_2 is not this simple, with features such as cation vacancies, metal ion impurities and microtwinning all being common [1]. In fact, an entire range of materials fall into the γ-MnO_2 category. This is, however, beyond the scope of the present work, since a single EMD sample was used throughout.

The currently accepted reduction mechanism for EMD is based on the work of Kozawa et al. [2–7], and further developed by Tye et al. [8–15], Swinkels et al. [16], Chabre and Pannetier [1] and Donne et al. [17–19]. The reduction can be divided into two stages:

(i) Homogeneous reduction ($MnO_{2.0}$ to $MnO_{1.5}$ (MnOOH)) in which electrons from the external circuit are inserted into the EMD structure, causing the reduction of Mn^{4+} ions to Mn^{3+} ions. For charge neutrality, a proton from water decomposition in the electrolyte, is also inserted. The proton is located on an O^{2-} ion (to form OH^-) adjacent to the Mn^{3+} ion. This is

a homogeneous process since the only change that occurs is a lattice expansion due to the larger ionic radii of the reduced species. This stage can be described by

$$\mathrm{MnOOH}_r + \Delta\mathrm{H_2O} + \Delta\mathrm{e}^- \rightarrow \mathrm{MnOOH}_{r+\Delta} + \Delta\mathrm{OH}^- \quad (0 \leqslant r + \Delta \leqslant 1) \tag{1}$$

where r is the initial moles of hydrogen in the EMD structure ($r \approx 0.1$ in an unreduced EMD) and Δ is the moles of protons and electrons inserted into the EMD structure during reduction. This stage of reduction is complicated by the presence of Mn^{4+} ions located in different structural domains that are reduced at different potentials. This is the main power generation stage for the EMD electrode.

(ii) Heterogeneous reduction ($MnO_{1.5}$ (MnOOH) to $MnO_{1.0}$ ($Mn(OH)_2$)) involving a phase transition that can be described by

$$\mathrm{MnOOH} + \mathrm{H_2O} + \mathrm{e}^- \rightarrow \mathrm{Mn(OH)_2} + \mathrm{OH}^- \tag{2}$$

The potential at which this stage occurs is too low to be of significance, and in fact the observation of heterogeneous reduction usually signifies the end of the useful life of the EMD electrode. Rechargeable alkaline Zn/MnO_2 cells, such as those marketed by Rayovac, avoid this stage by lowering the anode to cathode ratio in the cell; i.e., an anode limited cell. This stage will not be considered further in this study.

In a previous study [20], electrochemical impedance spectroscopy (EIS) was used to investigate the behavior of the alkaline EMD electrode under a variety of experimental conditions. The experimental data from this study were interpreted using an equivalent circuit derived from an understanding of the physical and electrochemical processes occurring within the electrode. This technique of data interpretation was somewhat successful but some of the equivalent circuit parameters necessary for a good fit between the experimental and predicted data were not readily interpretable in terms of the physical picture of the electrode.

It should be pointed out that the electrodes used for this EIS study were quite porous, and so an alternative approach to data interpretation is to use a transmission line to represent the electrode. The work by Newman and Tobias [21] is an early example of the application of a transmission line model to the current distribution in a porous electrode, while the work by Song et al. [22, 23], who developed a transmission line model to consider the pore size distribution of a gold powder electrode, is a more recent example. Of more relevance to this work is that by Atlung and Jacobsen [24] who used a transmission line to model EIS data obtained on a γ-MnO_2 sample dispersed in an aqueous KCl/KOH electrolyte. The experimental design used by these authors involved electrolyte flooded conditions, which are somewhat different from those used in a commercial EMD electrode. Therefore, it is the purpose of this study to develop a transmission line model that better represents the experimental conditions found in a commercial EMD electrode. Data predicted from the model will then be compared with selected experimental data obtained in the previous study [20].

2. Experimental

The experimental techniques and apparatus used to carry out the EIS experiments have been described in detail elsewhere [20]. Briefly, there are four areas of importance.

2.1. *Blackmix preparation*

All electrodes were prepared from blackmixes consisting of appropriate proportions of EMD and electrolyte. Commercial EMD electrodes contain graphite; however, graphite was excluded here to avoid the low resistivity path that it creates, and hence focus on the EMD/electrolyte interface.

2.2. *Electrochemical cell*

The cell consists of a reinforced teflon tube, in which an EMD blackmix was compressed between two stainless steel pistons to form the electrode. The pistons also act as current collectors for the passage of current through the cell.

2.3. *Apparatus*

A 5 mV RMS sinusoidal signal was applied to each electrode using a Solartron Instruments 1255 Frequency Response Analyzer and 1287 Electrochemical Interface. The frequency range covered was from 60 kHz to 0.1 Hz.

2.4. *Numerical analysis*

To compare experimental data with data predicted from the transmission line model, a complex non-linear least squares refinement procedure was adopted [25, 26]. It involved simultaneously fitting the real and imaginary components of the predicted impedance ($Z_i(\omega) = Z_i'(\omega) + \mathrm{j}Z_i''(\omega)$) using the expression

$$S = \sum_i w_i \left[\{Z_i' - Z_i'(\omega)\}^2 + \{Z_i'' - Z_i''(\omega)\}^2 \right] \tag{3}$$

where S is indicative of the divergence between experimental and predicted data, $Z_i = Z_i' + \mathrm{j}Z_i''$ is the experimental data set and w_i is a weighting factor given by

$$w_i = \frac{1}{|Z_i|^2} \tag{4}$$

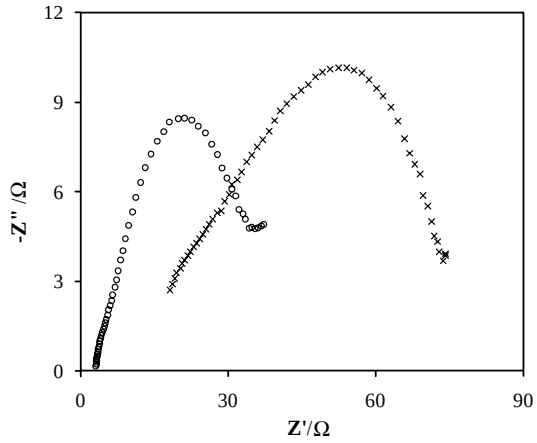

Fig. 1. Nyquist plot of typical EIS experiments on the EMD electrode: (○) EMD + ~10% 9.0 M KOH and (×) EMD + ~5% 9.0 M KOH. Compaction pressure 2.3×10^3 kg; electrode thickness 0.200 cm; 60 kHz–0.1 Hz. %.

The fitting procedure involved optimizing the transmission line parameters so as to minimize *S*.

3. Results

Numerous EIS experiments have been carried out on the EMD electrode to investigate the effects of electrode thickness, electrode compaction pressure, electrolyte content, electrolyte concentration, EMD oxidation state and the presence of TiO_2 (anatase) as an electrode additive. These results have been described in detail in a previous publication [20] and so will not be presented again. However, a examples, Figure 1 shows the Nyquist plots obtained from typical EIS experiments on the EMD electrode. Generally speaking, the EIS data consists of a very depressed and distorted semi-circular arc. The distortion at high frequencies was due to the presence of another overlapping semi-circle [20]. At low frequencies, the increase in the imaginary component was due to various diffusion processes within the electrode. To assist in interpreting this data the expressions describing the impedance of a transmission line will now be derived.

3.1. *Transmission line development*

The derivation that follows was based on the work initially carried out by de Levie [27–30], and used by Park and Macdonald [31] in the study of porous magnetite films on carbon steel.

In this study, an intimate mixture of EMD and aqueous KOH electrolyte was compressed between two stainless steel pistons in a reinforced teflon tube. A schematic of this arrangement is shown in Figure 2. This figure gives us the first indication of possible charge transport paths through the electrode; i.e., an electronic path through the manganese dioxide and an ionic path through the electrolyte. There is also the possibility of charge transfer across the interface between the solid and solution phases. With only manganese dioxide and electrolyte present in the cell, charge transfer at this interface depends on both the forward and reverse reactions in Equation 1. The sinusoidal voltage applied to the cell ensures different potentials within the electrode, although no net charge transfer occurs. Hence, those regions within the electrode at relatively negative potentials will be reduced, and correspondingly those at more positive potentials will be oxidized. Refining the picture of the electrode further leads to the block diagram shown in Figure 3. In this figure we have attempted to model the electrode based on a single electrolyte filled pore with uniform cross-section and length. This does neglect the tortuous nature of the electrolyte path through the electrode that was evident in Figure 2; however, this can be compensated for by assuming that the pore is longer than just the distance between the two current collectors. In describing the electrode this way we have also assumed that the potentials along the length of the pore can be replaced

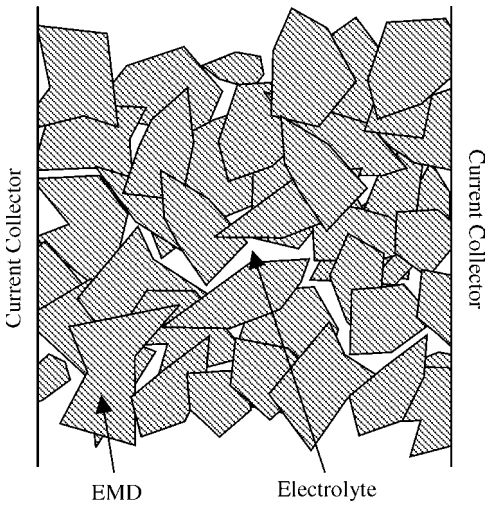

Fig. 2. Schematic diagram of the EMD electrode.

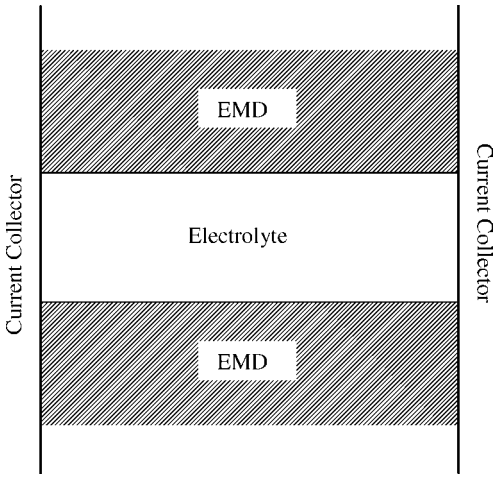

Fig. 3. Block diagram of the EMD electrode.

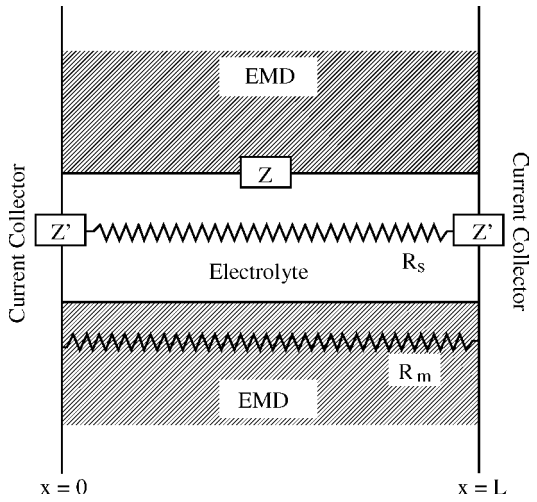

Fig. 4. Circuit elements assigned to the physical and electrochemical processes occurring in the EMD electrode. R_m is the EMD resistance per unit length of pore ($\Omega\ cm^{-1}$); R_s is the electrolyte resistance per unit length of pore ($\Omega\ cm^{-1}$); Z is the EMD/electrolyte interfacial impedance for unit length of pore (Ω cm); Z' is the current collector/electrode interfacial impedance at the pore ends (Ω); and x is the distance along the length of the pore (cm).

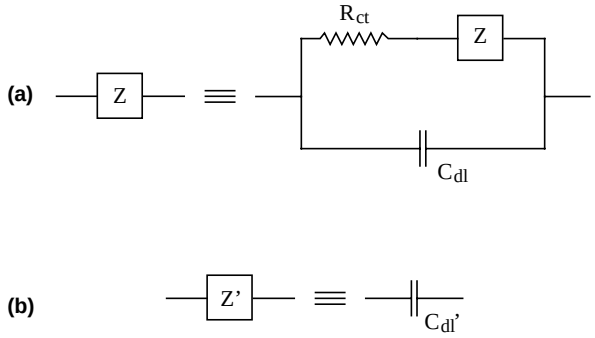

Fig. 5. Equivalent circuit representation of (a) the EMD/electrolyte interface and (b) the current collector/electrode interface.

by the average potential in the planes perpendicular to the pore axis. This assumption means that any curvature of the equipotential surfaces within the pore can be neglected; i.e., we have ignored the tortuous nature of the pore. This procedure has transformed the three-dimensional electrode into a one-dimensional problem.

The next stage in development is to assign circuit elements to the physical and electrochemical processes occurring within the electrode. The first step in achieving this is shown in Figure 4, where we have identified the electronic path through the EMD and the ionic path through the electrolyte by two separate ohmic resistances, R_m and R_s, respectively. The EMD/electrolyte interfacial impedance and the current collector/electrode interfacial impedance have both been represented by generalized impedances, Z and Z', respectively. These impedances are based on a consideration of the possible faradaic and non-faradaic electrochemical processes that can occur at each interface. A schematic of the EMD/electrolyte interfacial impedance (Z) is shown in Figure 5(a). The faradaic process that occurs at this interface is homogeneous proton and electron insertion and extraction, as described previously in Equation 1. In an equivalent circuit this process can be represented by a charge transfer resistance (R_{ct}), which is a measure of the reaction rate. In series with R_{ct} is an impedance due to mass transport limitations within the electrode. This impedance may be associated with proton and electron diffusion within the manganese dioxide and/or mass transport of water molecules to or from the surface of the manganese dioxide. It can be represented by a Warburg impedance (Z_W); i.e.,

$$Z_W = \frac{\sigma\omega^{-1/2}}{\sqrt{2}}(1 - j) \tag{5}$$

where σ is the Warburg prefactor, ω is the angular frequency (rad s^{-1}) and $j = \sqrt{-1}$. In parallel with R_{ct} and Z_W is the non-faradaic branch of the interfacial impedance. This branch consists of a capacitance (C_{dl}) used to represent the behavior of the ionic double-layer at the EMD/electrolyte interface.

At the current collector/electrode interface there are two areas that have to be considered. The first is the electronic contact between the current collector and the EMD. For the purposes of this treatment, we have assumed that this is an ohmic contact that occurs with negligible resistance. The second area is the interface between the current collector and the electrolyte. The impedance of this interface is determined in part by the amplitude of the sinusoidal signal applied during the EIS experiment, since this will determine what occurs at this interface. During this study, a small amplitude sinusoidal signal (5 mV RMS) was applied between the current collectors and so no faradaic processes could occur at this interface. However, non-faradaic charging of the double-layer can occur and so the impedance of the current collector/electrode interface (Z') can be represented by a capacitance, as shown in Figure 5(b). This was confirmed experimentally through the use of electrolyte soaked separator paper only between the stainless steel pistons. The result was characteristic of a capacitor, with negligible contribution from faradaic reactions (e.g., corrosion) suggesting that within the time frame of our experiments the interface between the current collector and electrolyte was purely capacitive in nature.

Our picture of the EMD electrode can now be represented in discretized form, as shown in Figure 6. In this figure, i is the total current flowing through the electrode, while i_m and i_s are the currents flowing through the EMD and electrolyte phases, respectively. Analyzing this circuit using Ohm's and Kirchoff's laws leads to the following relationships:

$$i = i_m + i_s \tag{6}$$

$$-d\phi_m = i_m R_m\, dx \tag{7}$$

$$-d\phi_s = i_s R_s\, dx \tag{8}$$

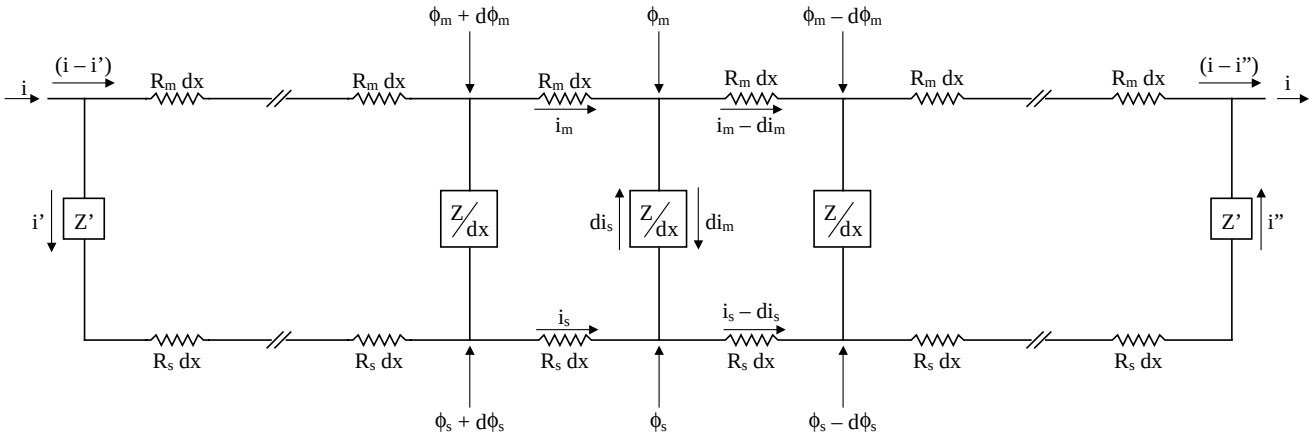

Fig. 6. Discretized form of the transmission line representing the EMD electrode.

$$(\phi_m - \phi_s) = -Z\left(\frac{di_m}{dx}\right) = Z\left(\frac{di_s}{dx}\right) \tag{9}$$

where ϕ_A represents the potential of phase A. Rearranging Equations 6–9 and assuming that Z, R_m and R_s are independent of x leads to

$$\frac{d^2(i_m)}{dx^2} - \gamma^2(i_m) = -\frac{R_s}{Z}i \tag{10}$$

$$\frac{d^2(i_s)}{dx^2} - \gamma^2(i_s) = -\frac{R_m}{Z}i \tag{11}$$

$$\frac{d^2(\phi_m - \phi_s)}{dx^2} - \gamma^2(\phi_m - \phi_s) = 0 \tag{12}$$

where

$$\gamma^2 = \frac{R_m + R_s}{Z} \tag{13}$$

Equations 10–12 are second order differential equations in i_m, i_s and $(\phi_m - \phi_s)$, respectively, that must be solved according to the following boundary conditions:

$$\begin{array}{llll} x = 0 & (\phi_m - \phi_s) = i'Z' & i_m = i - i' & i_s = i' \\ x = L & (\phi_m - \phi_s) = -i''Z' & i_m = i - i'' & i_s = i'' \end{array}$$

Therefore, the solutions are:

$$i_m = A_1 e^{\gamma x} + B_1 e^{-\gamma x} + \frac{R_s}{R_m + R_s}i \tag{14}$$

where

$$A_1 = \frac{iR_m(1 - e^{-\gamma L}) - (i'' - i'e^{-\gamma L})(R_m + R_s)}{2(R_m + R_s)\sinh(\gamma L)}$$

$$B_1 = \frac{-iR_m(1 - e^{\gamma L}) + (i'' - i'e^{\gamma L})(R_m + R_s)}{2(R_m + R_s)\sinh(\gamma L)}$$

and

$$i_s = A_2 e^{\gamma x} + B_2 e^{-\gamma x} + \frac{R_m}{R_m + R_s}i \tag{15}$$

where

$$A_2 = \frac{-iR_m(1 - e^{-\gamma L}) + (i'' - i'e^{-\gamma L})(R_m + R_s)}{2(R_m + R_s)\sinh(\gamma L)}$$

$$B_2 = \frac{iR_m(1 - e^{\gamma L}) - (i'' - i'e^{\gamma L})(R_m + R_s)}{2(R_m + R_s)\sinh(\gamma L)}$$

and

$$(\phi_m - \phi_s) = A_3 e^{\gamma x} + B_3 e^{-\gamma x} \tag{16}$$

where

$$A_3 = \frac{-Z'(i'' + i'e^{-\gamma L})}{2\sinh(\gamma L)}$$

$$B_3 = \frac{Z'(i'' + i'e^{\gamma L})}{2\sinh(\gamma L)}$$

Based on the transmission line shown in Figure 6, the potential drop across the electrode (V) is given by

$$V = (\phi_m - \phi_s)_{x=0} + \int_0^L i_s R_s \, dx - (\phi_m - \phi_s)_{x=L}$$

$$= \int_0^L i_m R_m \, dx = iZ_p \tag{17}$$

where Z_p is the total impedance of a single one-dimensional pore. From Equation 17,

$$(i'' + i') = \frac{2iR_m\{\cosh(\gamma L) - 1\}}{Z'\gamma\sinh(\gamma L) + (R_m + R_s)\{\cosh(\gamma L) - 1\}} \tag{18}$$

and hence

$$Z_p = \frac{\{2Z'R_m^2 + R_mR_sL(R_m + R_s)\}\{\cosh(\gamma L) - 1\} + Z'\gamma R_mR_sL\sinh(\gamma L)}{Z'\gamma(R_m + R_s)\sinh(\gamma L) + (R_m + R_s)^2\{\cosh(\gamma L) - 1\}} \quad (19)$$

Equation (19) represents the impedance of a single one-dimensional uniform pore. If we now assume that the electrode is composed of a network of single pores then the overall electrode impedance can be determined. To achieve this we need to define ρ_m and ρ_s, which are the specific resistivities (Ω cm) of the EMD and electrolyte phases, respectively; A, which is the current collector/electrode interfacial area (cm^2); n, which is the number of pores in the electrode; and, θ, which is the fraction of A covered by EMD. Therefore,

$$R_m = n\frac{\rho_m}{\theta A} \quad (\Omega\,cm^{-1}) \quad (20)$$

Electrolyte resistance per pore $= n\frac{\rho_s L}{(1-\theta)A}$ (Ω)

$$R_s = n\frac{\rho_m}{(1-\theta)A} \quad (\Omega\,cm^{-1}) \quad (21)$$

Now, the total area of pores in the electrode is $(1-\theta)A$ cm^2 and so assuming uniform cylindrical pores,

$$\text{Area per pore} = \frac{(1-\theta)A}{n} \quad (cm^2)$$

and therefore,

$$\text{Pore radius } (r) = \frac{(1-\theta)^{1/2}A^{1/2}}{(n\pi)^{1/2}} \quad (cm)$$

Letting the specific impedances (Ω cm^2) of the pore wall and pore base be Z_{wall} and Z_{base}, respectively, then

$$\text{Pore wall impedance per pore} = \frac{Z_{wall}}{2\pi rL} = Z_{wall}\frac{n^{1/2}}{2\pi^{1/2}(1-\theta)^{1/2}A^{1/2}L} \quad (\Omega)$$

That is,

$$Z = Z_{wall}\frac{n^{1/2}}{2\pi^{1/2}(1-\theta)^{1/2}A^{1/2}} \quad (\Omega\,cm) \quad (22)$$

Similarly,

$$\text{Pore base impedance per pore} = \frac{Z_{base}}{\pi r^2} = Z_{base}\frac{n}{(1-\theta)A} \quad (\Omega)$$

Therefore,

$$Z' = 2Z_{base}\frac{n}{(1-\theta)A} \quad (\Omega) \quad (23)$$

Expressions for Z_{wall} and Z_{base} were determined from the equivalent circuits shown in Figure 5.

Since the pores in each electrode are in parallel, the total impedance of the electrode (Z_t) is,

$$\frac{1}{Z_t} = \frac{n}{Z_p}$$

or

$$Z_t = \frac{Z_p}{n} \quad (24)$$

where Z_p is the total impedance of a single uniform one-dimensional pore as given by Equations 19, taking into consideration Equations 22 and 23.

From the above derivation the impedance of the EMD electrode is a function of various electrical, electrochemical and geometric electrode properties. The goal of this paper is to use the transmission line as a model for our previously recorded EIS data. However, before the modeling is carried out, it would be appropriate to observe how various transmission line parameters affect the resultant impedance. To achieve this we have calculated the transmission line impedance using arbitrary values for each of the parameters. Figure 7(a)–(h) shows the effects of changing each parameter on the resultant impedance. This figure shows that there are some general similarities between the EIS data predicted from the transmission line and the examples of experimental data shown in Figure 1. The most obvious are the presence of two distorted and depressed semi-circles at high frequencies, and a small diffusion tail at low frequencies. These features common to both the predicted and experimental data suggested that with some parameter refinement the transmission line model will be ideal for modeling the experimental EIS data.

Each of the transmission line parameters examined in Figure 7 has an effect on either the geometric, electrochemical or electrical properties of the electrode. Figure 7(a) and (b) shows the effect of the number of pores (n) and the surface coverage (θ) on the resultant impedance. Both n and θ are geometric parameters that influence the size and distribution of electrolyte filled pores within the electrode. For a fixed value of θ, increasing the number of pores in the electrode has the effect of decreasing the average pore diameter, which

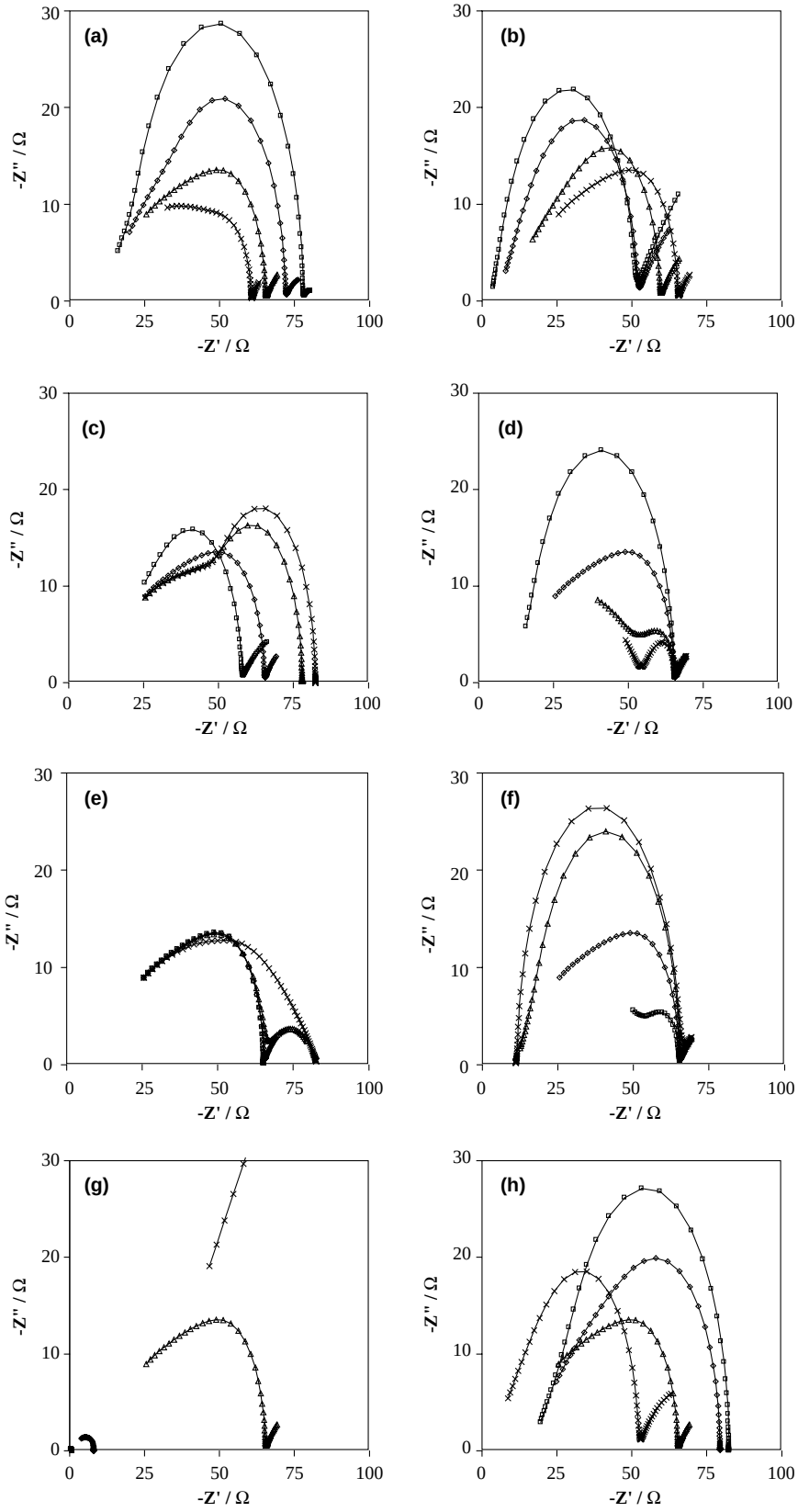

Fig. 7. Nyquist plots showing the impedance calculated from the transmission line as a function of various electrode parameters. (a) Number of pores (n): (□) 10; (◇) 100; (△) 1000; (×) 10000; (b) Surface coverage (θ): (□) 0.5; (◇) 0.75; (△) 0.9; (×) 0.95; (c) Pore wall charge transfer resistance (R_{ct}): (□) 1; (◇) 10; (△) 100; (×) 1000 Ω cm^2; (d) Pore wall double layer capacitance (C_{dl}): (□) 1; (◇) 10; (△) 100; (×) 1000 μF cm^{-2}; (e) Warburg prefactor (σ): (□) 1; (◇) 10; (△) 100; (×) 1000 Ω s$^{-1/2}$; (f) Pore base double-layer capacitance (C'_{dl}): (□) 1; (◇) 10; (△) 100; (×) 1000 μF cm^{-2}; (g) ρ_m/ρ_s ratio (changing ρ_m): (□) 0.1; (◇) 1; (△) 10; (×) 100 and (h) ρ_m/ρ_s ratio (changing ρ_s): (□) 0.1; (◇) 1; (△) 10; (×) 100.

leads consequently to an increase in the EMD/electrolyte interfacial area. With an increase in this interfacial area, more emphasis will be placed on the processes occurring at this interface, relative to the electrolyte/current collector interface at the pore base, when determining the overall impedance. In a similar fashion, increasing the degree of EMD surface coverage, for a fixed number of pores, has the effect of decreasing the average pore diameter. However, unlike the number of pores, increasing the surface coverage leads to a decrease in the EMD/electrolyte interfacial area. Hence the EMD/electrolyte interfacial impedance will be lowered with respect to the electrolyte/current collector impedance at the base of the pore. Furthermore, both n and θ seem to have more of an effect on the behavior of the lower frequency semi-circle in the EIS data.

The effects of pore wall charge transfer resistance (R_{ct}), pore wall double-layer capacitance (C_{dl}), Warburg prefactor (σ) and the pore base double-layer capacitance (C'_{dl}) are shown in Figure 7(c)–(f). These parameters are directly related to the electrochemical processes occurring within the electrode. Let us first consider the EMD/electrolyte interfacial impedance which is determined by R_{ct}, C_{dl} and σ. Changing the impedance of this interface affects the amount of charge passing through the EMD and electrolyte phases. For instance, if the EMD/electrolyte interfacial impedance was very high, then very little charge would be involved with the interface and so the electrode would behave like two distinct resistances in parallel. Conversely, if the impedance of the EMD/electrolyte interface were low, any charge in the electrode would be transferred across the interface to the phase with the lowest resistivity, and so the electrode would then behave like a single resistance. In this study, however, the impedance of the EMD/electrolyte interface was not so large or small that it did not play a significant role in determining the overall electrode impedance.

The relative values of R_{ct}, C_{dl} and σ determine the extent of faradaic and non-faradaic processes occurring at the EMD/electrolyte interface. An increasing value of R_{ct} (Figure 7(c)) implies that the faradaic charge transfer reaction (Equation 1) is becoming slower, and hence it is not surprising that the resulting impedance increases, particularly at low frequencies. The effects of mass transport on the faradaic charge transfer reaction, and hence the overall impedance, are manifest through the Warburg prefactor (σ), which is inversely related to the square root of the diffusion coefficient of electroactive species within the EMD of electrolyte. Therefore, increasing σ means that the mass transport of electroactive species to the EMD/electrolyte interface is slower, and hence the electrode impedance should increase. This situation was observed in Figure 7(e), particularly for the low frequency semi-circle. The non-faradaic processes at the EMD/electrolyte interface are represented by C_{dl}. Changing C_{dl} also has a significant effect on the overall electrode impedance, particularly the low frequency semi-circle. Figure 7(d) shows that an increase in C_{dl} dramatically reduces the imaginary component of the electrode impedance. This was to be expected, given that the impedance of a capacitor is inversely proportional to its capacitance.

The electrochemical processes occurring at the electrolyte/current collector interface have been represented by C'_{dl}, the pore base double-layer capacitance. Non-faradaic charging of the double layer is the only process occurring at this interface due to the small amplitude sinusoidal signal used in these experiments. The impedance of the pore base influences the amount of charge that passes through the EMD/electrolyte interface. For instance, if the pore base impedance were large, then the majority of charge passing through the electrode in the electrolyte will pass through the EMD/electrolyte interface and eventually through the EMD/current collector interface. Alternatively, if the pore base impedance were small, then very little charge would be passed through the EMD/electrolyte interface because now the impedance of the EMD/current collector and electrolyte/current collector interfaces are comparable. Figure 7(f) shows that increasing C'_{dl} leads to an increase in the imaginary component of the impedance, particularly that associated with the low frequency semi-circle.

Examples of the effect of changing the resistivities of the EMD (ρ_m) and electrolyte (ρ_s) phases on the overall electrode impedance are shown in Figure 7(g) and (h), respectively. The data in these figures was obtained by changing ρ_m or ρ_s in the ratio ρ_m/ρ_s. These resistivities represent the electrical properties of the electrode, and they determine the amount of charge passing through the EMD and electrolyte phases. For example, if the ρ_m/ρ_s ratio were large, and assuming a relatively small EMD/electrolyte interfacial impedance, then most of the charge would pass through the electrode in the lower resistance electrolyte phase. Alternatively, if the ratio ρ_m/ρ_s were small, then most of the charge would pass through the electrode in the EMD phase. The charge passing through each phase also depends on the EMD/electrolyte interfacial impedance, since charge passing through the electrode must be able to change to the least resistive phase.

Figure 7(g) shows that increasing the ρ_m/ρ_s ratio by changing ρ_m dramatically increases the electrode impedance. This result was to be expected given that the electrodes under study were composed mainly of EMD, and hence the majority of charge passed through the electrode was in this phase. Therefore, increasing the resistivity of this phase should lead to an increase in the overall electrode impedance. Figure 7(h) shows that the effects of changing ρ_s in the ratio ρ_m/ρ_s are more complicated. Increasing ρ_m/ρ_s by changing ρ_s means that ρ_s must decrease, and Figure 7(h) shows that this leads to an overall decrease in the electrode impedance, though not in a linear fashion. Under these conditions, it seems that decreasing ρ_s leads to a reduction in the impedance of the low frequency semi-circle and an increase in the impedance of the high frequency semi-circle. The cause of this may be due to an increase in the

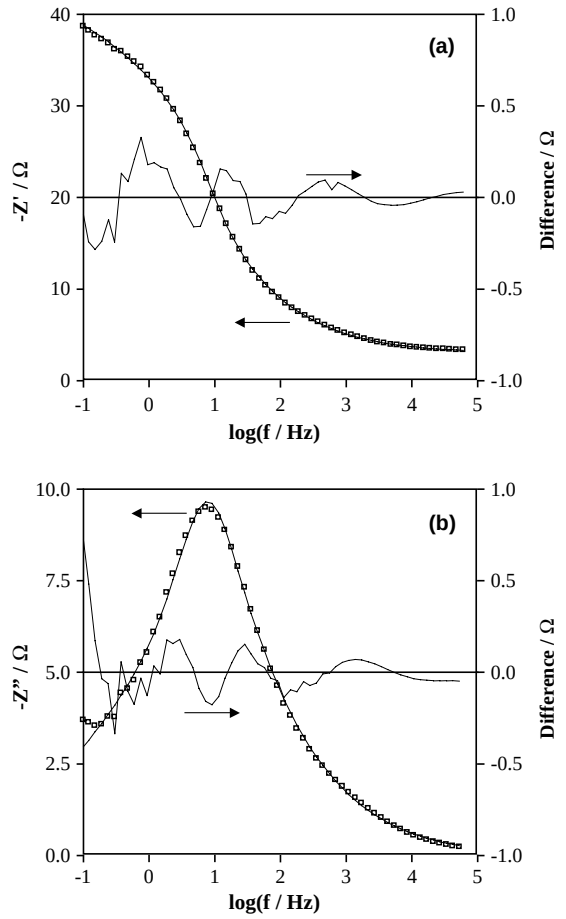

Fig. 8. Example of the comparison between experimental EIS data (cf. Figure 1) and data predicted from the transmission line model: (□) experimental data.

amount of charge passing through the EMD/electrolyte interface and hence more charge passing through the electrode in the electrolyte phase.

3.2. *Data modeling*

The mathematical expressions developed for the transmission line in the previous section were then modeled to experimental EIS data obtained in a previous study, using the complex non-linear least squares (CNLS) regression approach outlined in the Experimental section. As an example, the experimental data shown in Figure 1 was modeled using the transmission line. Figure 8 is a typical example showing the difference between the predicted and experimental impedance data, while Table 1 shows the transmission line parameters derived from the CNLS fitting procedure. Clearly the transmission line is a good model for interpreting the EMD electrode behavior, with only ~3% deviation from the experimental EIS data (Figure 8) and a very small sum of the squares of the residuals (S in Table 1).

The examples of experimental EIS data in Figure 1 were obtained from EMD electrodes with varying proportions of 9.0 M KOH electrolyte. These examples were selected because the formation of natural pores within the EMD electrode is a critical feature of the transmission line model. To further confirm the suitability of the transmission line as a model for the EMD electrode it is appropriate that we confirm that the trends in parameter values obtained from the CNLS fitting procedure are valid in terms of our physical understanding of the electrode.

The faradaic processes occurring at the EMD/electrolyte interface in the transmission line model are represented by R_{ct}, σ and m. R_{ct} represents how facile Equation 1 is, while σ and m are representative of the mass transport properties of the electroactive species at the interface. The data in Table 1 (R_{ct}) suggests that the reaction described by Equation 1 was more facile in the electrode containing less electrolyte. However, what is of more importance is the overall impedance of the faradaic processes occurring at this interface. Under these circumstances the impedance of the faradaic processes in the electrode ($R_{ct} + Z_W$) with less electrolyte was much larger, particularly at lower frequencies. This was to be expected given the increase in tortuosity and hence length of the electrolyte path through the electrode as the electrolyte content was decreased. This result implies that mass transport of electroactive species in the electrolyte to the EMD surface is an important feature of EMD electrode behavior. It is also of particular relevance to EMD cathodes in alkaline Zn/MnO_2 cells since they operate typically under electrolyte starved conditions.

Probably the most dramatic changes that occur between the two sets of parameters are those of C_{dl} and C'_{dl}. In both cases Table 1 shows that there is a dramatic decrease in these parameters as the electrolyte content was decreased. This result was to be expected since C_{dl} and C'_{dl} are indicative of the EMD/electrolyte and electrolyte/current collector interfaces, respectively. With less electrolyte present the surface area of these interfaces would be much less, hence the lower values of C_{dl} and C'_{dl}. The addition of electrolyte to dry EMD leads, firstly, to the progressive filling of EMD pores. Therefore, in an electrode with only a small amount of electrolyte present, the electrolyte would be located within the EMD pores and hence may not be available

Table 1. Transmission line parameters derived for the experimental EIS data in Figure 1

Electrolyte content	R_{ct} /Ω cm^2	σ /Ω cm^2 s$^{-1/2}$	m	C_{dl} /μF	C'_{dl} /μF	ρ_m /Ω cm	ρ_s /Ω cm	n	θ	S
~5%	0.1	61.3	0.5	87	1	55.8	4.6	120	0.81	1×10^{-3}
~10%	5.8	26.2	0.5	2753	1532	43.6	6.0	375	0.80	1×10^{-3}

for electrochemical processes (i.e., low values of C_{dl} and C'_{dl}). With an increasing electrolyte content the EMD pores are progressively filled. Eventually all the pore space is filled with electrolyte, at which time the interparticle spaces begin to be filled with electrolyte. During this pore filling process the EMD/electrolyte and electrolyte/current collector interfacial areas increase and hence the dramatic increase in C_{dl} and C'_{dl}. It should be noted that the optimum electrolyte level, found through experience, is 8–10%.

The changes observed for the number of pores (n) and the degree of EMD surface coverage (θ) were also expected. With a larger proportion of electrolyte present, the number of electrolyte filled pores would be expected to increase, while the EMD surface coverage should decrease. These trends were observed in Table 1.

Some of the other trends (e.g., ρ_m and ρ_s) are not as easily explained and demonstrate the complexity of the EMD electrode. Clearly, continuing studies are needed to explain this electrode behavior.

4. Summary and conclusions

A model for describing the behavior of the EMD electrode in concentrated KOH electrolytes in EIS experiments has been developed. This model was based on an electrical transmission line that considered the possible charge transport paths through the electrode. In general, charge transport through an EMD electrode can occur through the EMD (electronic path) or through the electrolyte (ionic path). Faradaic and nonfaradaic processes occurring at the EMD/electrolyte and electrolyte/current collector interfaces were also considered and included in the model.

The model, therefore, consisted of parameters describing the electrical, electrochemical and geometric properties of the electrode. Arbitrary values for these parameters were selected and used to calculate the electrode impedance over a wide frequency range. The trends expected from our physical picture of the electrode were observed in the resultant Nyquist plots of the EIS data.

Experimental EIS data taken from a previous study were then modeled using the transmission line. At worst, there was less than 3% deviation between the experimental and predicted data, leading to the conclusion that the transmission line is an excellent model for describing the EIS behavior of the EMD electrode.

Acknowledgement

The authors would like to acknowledge the financial and technical support made available by Eveready Battery Company, Inc.

References

1. Y. Chabre and J. Pannetier, *Prog. Solid State Chem.* **23** (1995) 1.
2. A. Kozawa and J.F. Yeager, *J. Electrochem. Soc.* **112** (1965) 959.
3. A. Kozawa, T. Kalnoki-Kis and J.F. Yeager, *J. Electrochem. Soc.* **113** (1966) 405.
4. A. Kozawa and R.A. Powers, *J. Electrochem. Soc.* **113** (1966) 870.
5. A. Kozawa and R.A. Powers, *Electrochem. Technol.* **5** (1967) 535.
6. A. Kozawa and R.A. Powers, *J. Electrochem. Soc.* **115** (1968) 122.
7. A. Kozawa and J.F. Yeager, *J. Electrochem. Soc.* **115** (1968) 1003.
8. W.C. Maskell, J.E.A. Shaw and F.L. Tye, *J. Appl. Electrochem.* **12** (1982) 101.
9. W.C. Maskell, J.E.A. Shaw and F.L. Tye, *Electrochim. Acta* **26** (1981) 1403.
10. W.C. Maskell, J.E.A. Shaw and F.L. Tye, *Electrochim. Acta* **27** (1982) 425.
11. W.C. Maskell, J.E.A. Shaw and F.L. Tye, *J. Power Sources* **8** (1982) 113.
12. W.C. Maskell, J.E.A. Shaw and F.L. Tye, *Electrochim. Acta* **28** (1983) 225.
13. W.C. Maskell, J.E.A. Shaw and F.L. Tye, *Electrochim. Acta* **28** (1983) 231.
14. F.L. Tye, *Electrochim. Acta* **30** (1985) 17.
15. F.L. Tye and S.W. Tye, *J. Appl. Electrochem.* **25** (1995) 425.
16. D.A.J. Swinkels, K.E. Anthony, P.M. Fredericks and P.R. Osborn, *J. Electroanal. Chem.* **168** (1984) 433.
17. S.W. Donne, G.A. Lawrance and D.A.J. Swinkels, *J. Electrochem. Soc.* **144** (1997) 2949.
18. S.W. Donne, G.A. Lawrance and D.A.J. Swinkels, *J. Electrochem. Soc.* **144** (1997) 2954.
19. S.W. Donne, G.A. Lawrance and D.A.J. Swinkels, *J. Electrochem. Soc.* **144** (1997) 2961.
20. S.W. Donne and J.H. Kennedy, *J. Appl. Electrochem.*, Accepted for publication.
21. J.S. Newman and C.W. Tobias, *J. Electrochem. Soc.* **109** (1962) 1183.
22. H.K. Song, Y.H. Jung, K.H. Lee and L.H. Dao, *Electrochim. Acta* **44** (1999) 3513.
23. H.K. Song, H.Y. Hwang, K.H. Lee and L.H. Dao, *Electrochim. Acta* **45** (2000) 2241.
24. S. Atlung and T. Jacobsen, *Electrochim. Acta* **21** (1976) 575.
25. B.A. Boukamp, *Solid State Ionics* **18** (1986) 136.
26. B.A. Boukamp, *Solid State Ionics* **20** (1986) 30.
27. R. de Levie, *Electrochim. Acta* **8** (1963) 751.
28. R. de Levie, *Electrochim. Acta* **9** (1964) 1231.
29. R. de Levie, *Electrochim. Acta* **10** (1965) 113.
30. R. de Levie, *Adv. Electrochem. Electrochem. Eng.* **6** (1967) 329.
31. J.R. Park and D.D. Macdonald, *Corros. Sci.* **23** (1983) 295.